Am J Transl Res 2019;11(10):6650-6659
www.ajtr.org /ISSN:1943-8141/AJTR0094974

Original Article

One-step strategy for cartilage repair using acellular bone matrix scaffold based in situ tissue engineering technique in a preclinical minipig model

Linghui Dai*, Zhenming He*, Yanfang Jiang, Xin Zhang, Shuang Ren, Jingxian Zhu, Zhenxing Shao, Hongjie Huang, Jiying Zhang, Xin Fu, Xiaoning Duan, Xiaoqing Hu, Yingfang Ao

*Institute of Sports Medicine, Peking University Third Hospital, Beijing Key Laboratory of Sports Injuries, 49 North Garden Road, Haidian District, Beijing 100191, PR China. *Equal contributors.*

Received April 7, 2019; Accepted August 5, 2019; Epub October 15, 2019; Published October 30, 2019

Abstract: Cartilage defects are most commonly seen in the knee joint. However, due to the limited self-recovery ability of cartilage, the repair of articular cartilage defects is still a great challenge despite that various approaches have been proposed. We designed a strategy to induce cartilage repair using acellular bone matrix (ABM), thereby creating an appropriate microenvironment for the in-situ cells with an easy surgical application. An in vitro system demonstrated that the ABM scaffold could promote cell adhesion, growth, proliferation, and chondrogenesis of mesenchymal stem cells. This experiment was performed in a minipig cartilage repair model. The repaired tissue was hyaline-like cartilage according to the morphological and histological results. The mechanical properties of the repaired tissue were similar to those of normal cartilage. The integration of repaired tissue and normal tissue in the ABM+M group was better than those of other two groups. The ABM-based, one-stage, minimally invasive, in situ procedure for cartilage regeneration can potentially improve the treatment of articular cartilage defects.

Keywords: Cartilage repair, acellular bone matrix, translational medicine

Introduction

Articular cartilage is a vital structure for maintaining the normal function of a joint. Articular cartilage defects are common injuries with a reported prevalence of 63% in sedentary population [1] and more than 50% in professional athletes [2]. If left untreated, even minor lesions can cause progressive degeneration, thereby resulting in pain, joint dysfunction, and osteoarthritis due to its limited self-recovery ability [3].

Current treatments succeed in providing relief of symptoms. However, damaged articular tissues are not replaced with new tissue with the same biomechanical properties and long-term durability as normal hyaline cartilage. To date, a number of techniques have been studied and applied to the treatment of cartilage injury [4-8]. Among these methods, microfracture is a first-line treatment that is easy to perform and can relieve patient symptom; it allows the bone marrow stem cells and growth factors released in situ to participate in cartilage repair. However, it is only effective for small-size lesions and always leads to the regeneration of fibrocartilage instead of hyaline cartilage [9-11]. Autologous chondrocyte implantation, even if it is able to regenerate hyaline-like cartilage [12, 13], requires a two-stage procedure with high operative risk, low cost-effectiveness, donor site morbidity, and relative longer recovery process [14-16]. These problems are shared by other transplantation techniques, such as osteochondral transplantation [17] and matrix-assisted chondrocyte implantation [18, 19]; these issues greatly limit the application of these techniques in the clinic.

Collectively, there are two main problems with the current methods. The first and most important problem is that the defect area lacks effective biologically active ingredients (cells and/or scaffold), thereby always leading to scar tissue or fibrous tissue repair. The second problem is

the lack of an effective induction for chondrocytes or cartilage tissue. The existing treatments on cartilage repair do not have the appropriate microenvironment for cartilage regeneration.

We designed a strategy that creates an appropriate microenvironment for the in-situ cells by a bioscaffold - the acellular bone matrix (ABM) - to induce cartilage repair. In our previous studies, we reported the methods that combined the Microfracture technique and decalcified bone matrix scaffold to regenerate hyaline-like cartilage in a single-step procedure in a rabbit model [20-22]. In the present study, a large animal (minipig) model were used to evaluate the safety and performance of the ABM scaffold with microfracture technique for the treatment of articular cartilage defects. It is a one-stage, minimally-invasive, in situ procedure for cartilage regeneration and is easy to adopt to clinical application.

Methods

Scaffold preparation

The ABM scaffolds were obtained from the iliac bone of allogeneic pigs. The scaffold was demineralized and decellularized by soaking in 0.5 M ethylenediaminetetraacetic acid (EDTA) at 4°C and pH 8.3. A fresh solution was used daily. The replaced EDTA solution was analyzed by atomic absorption spectrophotometry to track the demineralization process. The scaffolds were well demineralized after approximately 14 days. The decalcified scaffolds were stored at -80°C.

Chondrogenic differentiation of MSCs

MSCs were isolated and expanded as described previously [23]. The chondrocytes were also harvested from the healthy cartilage of the minipig. The cells used in subsequent experiments were passage 3. For the cell seeding, the scaffolds were first cut into small pieces (5×5×5 mm) and then sterilized with cobalt-60 for 24 h, soaked in 75% alcohol for 2 h, washed in sterile phosphate-buffered saline (PBS) 3 times each for 10 min, and conditioned with DMEM overnight. To seed the scaffolds, a 20 mL cell suspension containing 1×10^5 MSCs was loaded onto the scaffold. After 1 hour for cell attachment, the seeded scaffolds were cultured in 1 mL DMEM containing 0.1 mM dexamethasone, 50 mg/mL ascorbate 2-phosphate, 40 mg/mL L-proline, 100 mg/mL sodium pyruvate, 1 ITS. Scaffolds were harvested at 3, 7, 14 and 21 days for analysis.

Sulfated GAG and DNA quantification

Scaffold samples (with or without cells) were digested for 16 h with papain cocktail (125 mg/mL of papain, 5 mM L-cysteine, 100 mM Na_2HPO_4, and 5 mM EDTA; pH 6.2) at 60°C for DNA and glycosaminoglycan (GAG) estimation. The DNA content was measured using the PicoGreen DNA assay kit (Invitrogen, Carlsbad, California, USA) as per the manufacturer's protocol. The sample (20 mL) was mixed with 200 mL of Quant-iT PicoGreen reagent (1:200 dilution). The excitation and emission wavelengths of 480 and 528 nm, respectively, were measured using a fluorimeter. Readings were compared with standard curves made from calf thymus DNA (Sigma, St Louis, Missouri, USA). The DNA content was normalized to scaffold wet weight.

Total sulfated GAG (sGAG) was estimated using the 1,9-dimethylmethylene blue (DMMB) assay. The sample (20 mL) was mixed with 200 mL of DMMB reagent, and the absorbance was read on a plate reader (MultiSkan Spectrum; Thermo, Waltham, Massachusetts, USA) at 525 nm. A standard curve was established from chondroitin-6-sulfate from shark (Sigma) to compare absorbance for the samples. Total sGAG was normalized to scaffold wet weight and total DNA content to avoid variation due to scaffold sizes and cell numbers.

Confocal microscopy

The scaffold samples (with cells) were washed thrice with PBS (pH 7.4) and incubated with 0.1% (w/v) acridine orange for 5 min. Images from stained scaffolds were obtained using a confocal laser scanning microscope (Leica SP2 inverted microscope; Leica, Mannheim, Germany) equipped with 488 nm lasers.

In vivo animal experiments

Animal studies were performed at our hospital and were approved by the ethics committee in accordance with the guidelines for the care and use of laboratory animals. Protocols were

approved by the local Institutional Animal Care and Use Committee and were performed in compliance with the Guide for the Care and Use of Laboratory Animals (National Academies Press, National Institutes of Health Publication No. 85-23, revised 1996; permission number 2010-0089). Eighteen minipigs (36 knees) weighing 2.5-3.0 kg and 4-6 months old were used for this part of the investigation. Minipigs were divided into three treatment groups, as follows: Microfracture alone (M group), ABM implantation alone (ABM group), and Microfracture combined with ABM implantation (ABM+M group).

Surgical procedures

The animals were anesthetized by intravenous injection of 10 mL of ethylcarbamate (0.2 g/mL). After shaving, disinfection, and draping, the knee was opened by a parapatellar anteromedial incision, and the patella was everted. Full-thickness articular defects 9 mm in diameter were created by corneal trephine in the trochlear groove of the distal femur without destroying the subchondral bone. The following procedures was then performed. (1) ABM scaffold preparation: to allow bone marrow to penetrate ABM, holes were drilled through the ABM with a 0.5 mm-diameter drill bit. The drilled ABM was made into a 9 mm-diameter cylinder by a corneal trephine. (2) Microfracture: Microfracture was made into the medullary cavity. (3) The scaffold was implanted into the defect by placing the cortical part of the scaffold in contact with the subchondral bone. All implants were placed at the same level with the surface of the adjacent cartilage. Wound closure was performed in layers. All the animals were kept in cages and had free access to food pellets and water. At 6, 12, and 24 weeks after surgery, the animals were sacrificed with an intravenous injection of pentobarbital at 1 mL/kg.

Histological assessment and staining of repaired tissue

After sacrifice, the distal portions of the femurs (six samples in three pigs in each group) were cut off and then fixed in 4% paraformaldehyde (pH 7.4) for 48 h at 4°C. The femurs were decalcified in 20% EDTA (pH 7.2) in PBS with 5% paraformaldehyde at 4°C. The decalcified specimens were trimmed, dehydrated in a graded ethanol series, and embedded in paraffin. Serial sections (8 μm thick) were cut in a sagittal manner through the center of the operative site and stained with hematoxylin and eosin and toluidine blue. Immunohistochemistry was performed with type II collagen antibody (Abcam, Cambridge, UK).

Scanning electron microscopy

The repaired tissues were harvested 24 weeks from the surface of the implant in the trochlear groove of the right distal femur. The samples were fixed immediately in a mixture of 4 mL 25% glutaraldehyde and 96 mL 10 mmol/L Tris-HCl (pH 7.4) at 4°C for 1 day. Then, they were dehydrated with a graded series of 70%, 80%, 90%, and 100% ethanol. Critical point drying was performed in liquid CO_2 at 37°C. The specimens were vacuum-coated with a 5 nm layer of gold in a high-vacuum gold spatter coater and then viewed with a scanning electron microscope (S-2500; Hitachi High-Technologies Co., Hitachi-Naka City, Japan).

Nanoindentation assessment of repaired tissue

The biomechanical analysis of the repaired tissues was performed using nanoindentation in accordance with reported methods. The samples (n=9 each group) were isolated from the central part of the repaired tissues. The normal hyaline cartilage samples (n=9) were isolated from the non-operated trochlear parts of the knee. Circumfluent PBS was used to maintain hydration of the samples at room temperature during testing.

All indentations were performed using the TriboIndenter (Hysitron Inc., Minneapolis, Minnesota, USA) with a 100 mm radius of a curvature conospherical diamond probe tip. For each indentation, the maximum indentation depth was set to 1000 nm. The sample was loaded within the first 10 s of the sample's surface coming in contact with the tips. The samples were held at the maximum depth for 2 s, and unloaded in the last 10 s of contact. The data analysis of nanoindentation was performed based on a reported method.

Statistical analysis

For statistical analysis, all results are expressed as mean ± standard deviation. The results from the same group were processed using the Student t test, whereas the results between

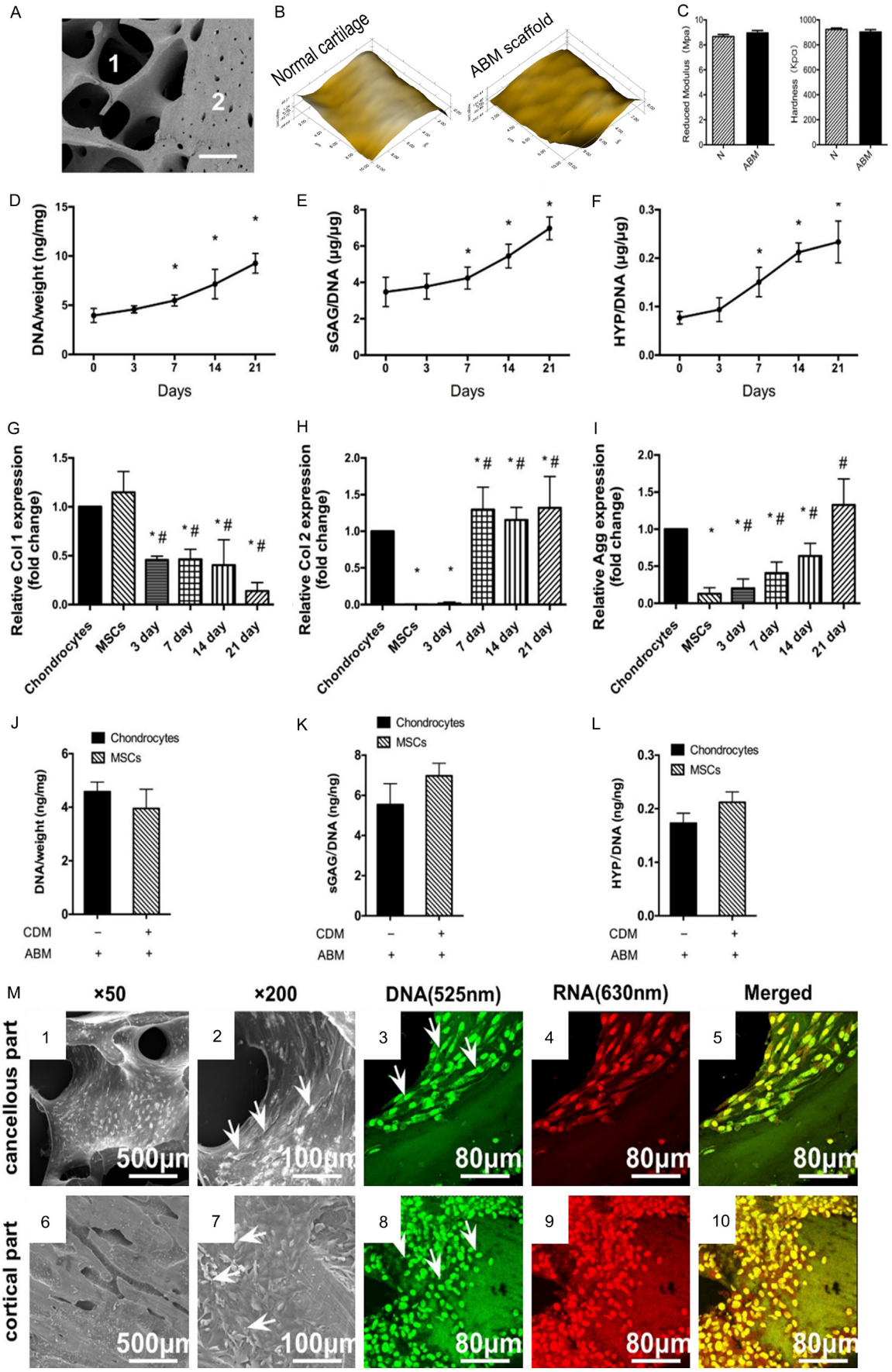
A
1
2
B
Normal cartilage
ABM scaffold
C
Reduced Modulus (Mpa)
Hardness (Kpa)
N
ABM
D
DNA/weight (ng/mg)
Days
E
sGAG/DNA (μg/μg)
Days
F
HYP/DNA (μg/μg)
Days
G
Relative Col 1 expression (fold change)
H
Relative Col 2 expression (fold change)
I
Relative Agg expression (fold change)
Chondrocytes
MSCs
3 day
7 day
14 day
21 day
J
DNA/weight (ng/mg)
K
sGAG/DNA (ng/ng)
L
HYP/DNA (ng/ng)
CDM
ABM
M
×50
×200
DNA(525nm)
RNA(630nm)
Merged
cancellous part
cortical part
500μm
100μm
80μm

Figure 1. The biomechanical properties of ABM scaffold and the in vitro cell growth, chondrogenesis and the cell attachment on ABM. (A) SEM image of The ABM scaffold. 1 indicate the cancellous part. 2 indicate the cortical part. (B) Microscopic geomorphology of normal cartilage and ABM surface was acquired during nanoindentation. (C) The reduced modulus and the hardness of normal cartilage and ABM were calculated during nanoindentation (n=6, *P<0.05). (D-F) MSCs were cultured in the ABM scaffold. DNA, GAG, and hydroxyproline contents were measured for over 21 days. (n=6, *P<0.05). (G-I). Expressions of collagen type I, collagen type II, and aggrecan for over 21 days. (n=6, *P<0.05 vs chondrocytes, $^{\#}$P<0.05 vs MSCs). DNA (J) GAG (K) and HYP (L) production by chondrocytes cultured alone in the ABM scaffold and MSCs cultured in ABM scaffold with chondrogenesis medium in vitro. (M) The attachment of MSCs on different parts of the ABM scaffold. Scanning electron microscopy images show the growth of MSCs on the surface of cancellous parts (1, 2) and cortical parts (6, 7) of the ABM at different magnifications (original magnification: 1 and 6: *200, 2, and 7: *500). Arrows indicate the typical cells grown on different parts of the scaffold. Confocal laser microscopic images show the growth of MSCs on the cancellous parts (3-5) of the ABM and the cortical parts (8-10). The MSCs grown on both parts of the scaffold were stained with green and red fluorescence uniformly (no apoptotic or necrotic cells). Green: the intercalated DNA stained by acridine orange with fluorescence at 515-545 nm. Red: the electrostatic RNA stained by acridine orange with fluorescence at 590-620 nm. Yellow: merged from (3 and 4) or (8 and 9). Magnification: *60.

groups were processed using analysis of variance (ANOVA). Processing was performed using the SPSS 17.0 statistical software (SPSS, Chicago, IL, USA). P<0.05 was considered statistically significant. All results were expressed as mean ± standard deviation.

Results

Chondrogenesis induction and biomechanical properties of ABM

The ABM scaffold is composed of two parts, the cortical part and the cancellous part (**Figure 1A**). This scaffold was made of decalcified bone matrix and was designed for easy clinical application. The ABM scaffold was porous (**Figure 1A**), and its surface was similar to that of normal cartilage (**Figure 1B**). It has natural ingredients appropriate for cell growth and cartilage induction. The reduced modulus and hardness of ABM were similar to those of normal cartilage according to the nanoindentation results (**Figure 1C**). Its biomechanical properties were better than those in normal cartilage, thereby indicating that the ABM scaffold will benefit early rehabilitation.

The ability of human bone marrow-derived mesenchymal stem cells (MSCs) to secrete cartilage matrix in this ABM scaffold was evaluated. At 21 days of in vitro culture, both DNA content (cell number), proteoglycan [secreted glycosaminoglycan (sGAG)] and collagen secreted (hydroxyproline, HYP) increased over a 21 day culture (**Figure 1D-F**). Gene expression supported the matrix production results (**Figure 1G-I**). Type I collagen expression decreased from 3 days, and the decreased level lasted for 21 days (**Figure 1G**). Type II collagen was increased from 7 days and reached a level similar to that of chondrocytes from 7 days to 21 days (**Figure 1H**). Aggrecan expression increased from 3 days to 21 days and reached a level similar to that of chondrocytes (**Figure 1I**). sGAG production by MSCs was comparable with that of mature chondrocytes that were cultured on the scaffold for 21 days without chondrogenesis medium. Both collagen production and sGAG production by the MSCs were similar to those of chondrocytes that were cultured for 21 days (**Figure 1J-L**).

The MSCs were well grown on both parts of the ABM scaffold according to images from the scanning electron microscope. The MSCs spread well (**Figure 1M6** and **1M7**) and adhered tightly to both the cancellous parts (**Figure 1M1** and **1M2**) and the cortical parts (**Figure 1M6** and **1M7**) of the scaffold, especially in the concave area of the ABM scaffold (**Figure 1M2** and **1M7**, as indicated by a white arrow).

Viability of MSCs grown on the ABM scaffold

The nuclei of MSCs grown on both cortical and cancellous parts were stained with green fluorescence uniformly (**Figure 1M3** and **1M8**), and results indicated living normal cells. All MSCs were stained with red fluorescence uniformly, thereby indicating that the cytoplasm of the MSCs was uniform, with no rupture and no apoptotic cells (**Figure 1M4** and **1M9**). No apoptotic or necrotic cells were seen on the images (**Figure 1M5** and **1M10**).

These in vitro results supported the potential of ABM scaffold, which benefits cell growth, and highlights the chondrogenesis potential of MSCs grown on scaffold in local cartilage repair.

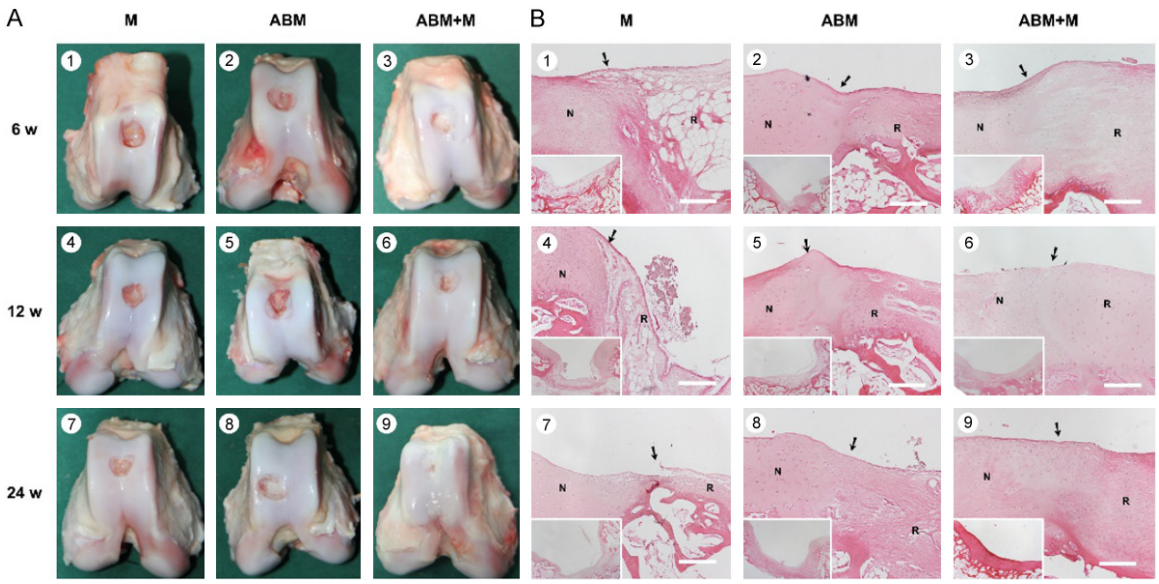

Figure 2. Cartilage repair with ABM scaffold in a porcine model. A. Macroscopic appearance of the cartilage defect healing in three groups at 6 (1-3), 12 (4-6), and 24 (7-9) weeks after the operation. The three groups were as follows: M group, cartilage defects were treated with the microfracture technique alone; ABM group, cartilage defects were implanted with ABM scaffold alone; and ABM+M group, cartilage defects were treated with microfracture and implanted with the ABM scaffold. B. H&E staining in the three groups after the operation. N, normal cartilage; R, repair tissues. The arrows indicate the margins of the normal tissue and the repaired tissue. Scale bars=500 μm.

Cartilage repair in a large-animal model

We previously performed animal (rabbit) studies to establish the cartilage repair potential of ABM scaffold homotransplantations and xenotransplantation. This one-step technique based on ABM scaffold successfully induced hyaline-like articular cartilage repair [20, 21].

Cartilage repair should be confirmed in large animal models to establish clinical guidelines for the surgical application of the ABM scaffold and the cartilage repair technique. Porcine chondral defects were subjected to the Microfracture technique alone in the M group and implanted with ABM scaffold alone in the ABM group. These defects were subjected to Microfracture and implanted with the ABM scaffold in ABM+M group.

Macroscopic findings of the repaired cartilage defects

Animals were sacrificed, and their knees were excised and examined at 6, 12, and 24 weeks after the operation. In the ABM+M group, full-thickness defects were repaired with glossy white tissue, which was comparable with normal articular cartilage in appearance, as shown in **Figure 2A3**, **2A6**, **2A9**. On the contrary, defects in the M group remained largely unfilled, as shown in **Figure 2A1**, **2A4**, **2A7**. Incomplete integration, an uneven surface, and thinner repair tissues were also observed in the ABM group, as shown in **Figure 2A2**, **2A5**, **2A8**. These microscopic findings were similar to previous findings in rabbit [20].

Histological findings of the repaired cartilage defects

Hyaline-like chondrocytes were seen in the ABM+M group in the repaired region, with good integration between repair tissue and normal cartilage. The tidemark was clear, as shown in **Figure 2B3**, **2B6**, **2B9**. The matrix production of repair tissue was close to that of normal cartilage, with dark toluidine blue (TB) staining and positive immunohistochemical (IHC) staining of Type II collagen, as shown in **Figure 3A3**, **3A6**, **3A9** and **3B3**, **3B6**, **3B9**. The repaired tissues in the M group were similar to scar or fiber tissue but with fewer cells, thinner repaired tissue, and poorer filling in the repaired region and with no clear tidemark, as shown in **Figure 2B1**, **2B4**, **2B7**. No staining or very light staining of TB and IHC staining were observed, as shown in **Figure 3A1**, **3A4**, **3A7** and **3B1**, **3B4**, **3B7**. Fewer hyaline-like chondrocytes were observed seen in the ABM group with thinner

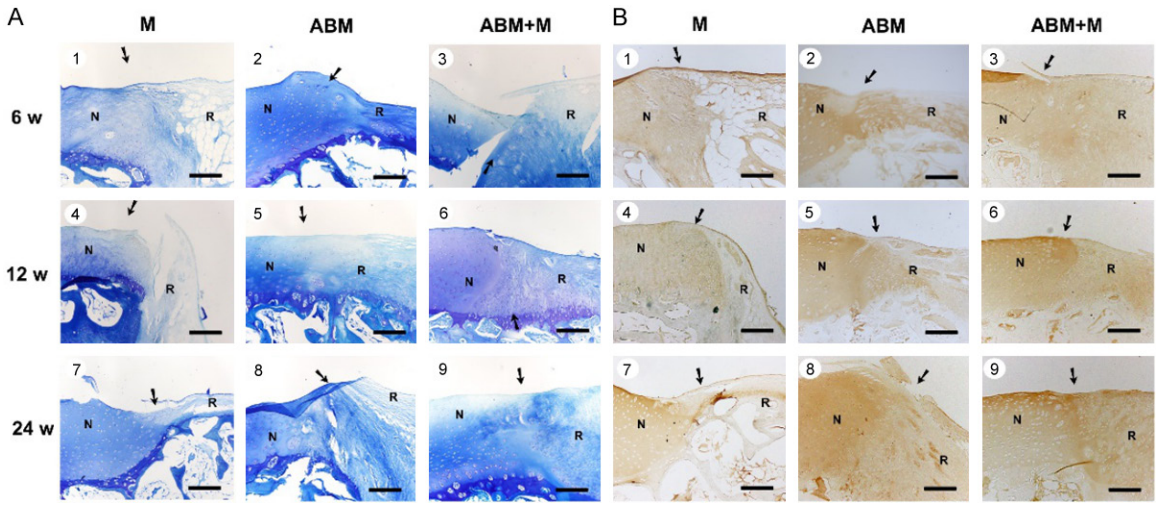

Figure 3. Toluidine blue staining and IHC staining of Type II collagen of repaired tissue and normal cartilage in the three groups at 6 (1-3), 12 (4-6), and 24 (7-9) weeks after the operation. ABM, decalcified cortical cancellous bone matrix; ABM+M, perforated ABM combined with microfracture; N, normal cartilage; R, repair tissues. The arrows indicate the margins of the normal tissue and the repaired tissue. Scale bars=500 μm.

repair tissue, incomplete filling in the repair region, and irregular tide mark, as shown in **Figure 2B2**, **2B5**, **2B8**, in comparison with the ABM+M group. Light TB and IHC staining was seen in the ABM group, as shown in **Figure 3A2**, **3A5**, **3A8** and **3B2**, **3B5**, **3B8**.

Surface integration and the biomechanical properties of the repaired cartilage defects

In the ABM+M group, the surface of the repaired tissues was smooth, at the same height of the normal cartilage (**Figure 4A4**), and better integrated with the surrounding cartilage compared with those of M or ABM groups (**Figure 4A2**, **4A3**). Clear cracks between the repaired and normal tissues were observed in the M and ABM groups, but the repair tissues in the ABM group were smoother than those in the M group.

Nanoindentation was performed to assess the biomechanical properties of the three groups at 24 weeks. The surface of repaired tissues in ABM+M group was well integrated and smooth, which was consistent with the results of the SEM analysis (**Figure 4B**). However, the surface of repaired tissues in the M and ABM groups were scraggier and rougher than normal cartilage (**Figure 4B**).

The reduced modulus, hardness, and contact stiffness are considered suitable measurement for comparing the mechanic properties of different repaired tissues. In our study, the normal cartilage showed the highest reduced modulus, followed in descending order of stiffness by the samples from ABM+M group, ABM group, and M group (**Figure 4C**). Similar results can be seen in the assessment of hardness and contact stiffness (**Figure 4D** and **4E**). Normal cartilage displayed the highest contact stiffness and reduced modulus and hardness, whereas the repaired tissues in the M group showed the lowest values among the four groups. Similar to native cartilage, the repaired tissue in the ABM+M group established a significantly higher reduced modulus, hardness and contact stiffness than those of the M and ABM groups (**Figure 4C-E**). This finding indicated that the biofunctional materials promoted well-organized cartilage repair, thereby resulting in biomechanical properties similar to those of normal cartilage.

Discussion

Cartilage repair is still a great challenge for clinicians and researchers. Various methods have been studied to promote cartilage repair, but no satisfactory method has been developed. There are still many problems, such as insufficient cell supply [11], new damage to the donor site [4], and chondrocyte dedifferentiation during its expansion in vitro [16]. Moreover, the patient always needs to undergo two operations to complete the treatment in some methods, such as ACI technique [12]. These problems also exist in other transplantation tech-

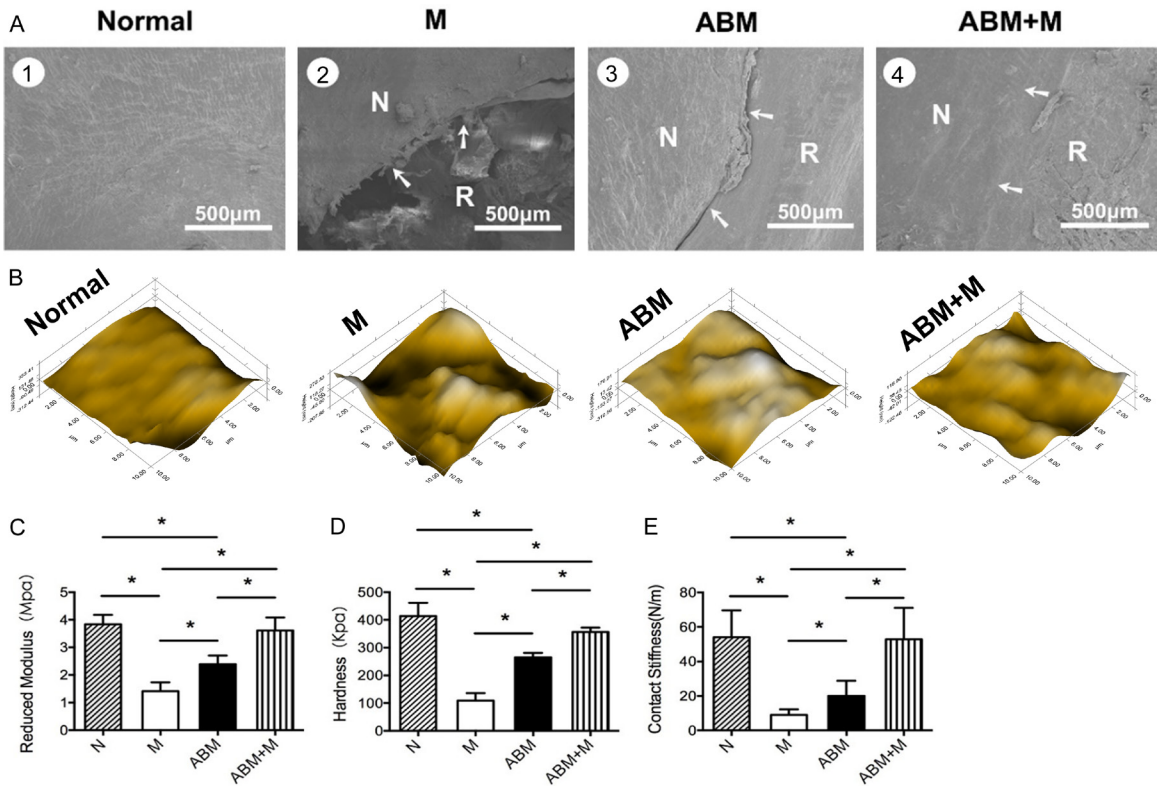

Figure 4. The integration and biomechanics properties of the repair tissue. Scanning electron microscopy images from 3 groups at 24 weeks after the operation (A). ABM, decalcified cortical-cancellous bone matrix; ABM+M, perforated ABM combined with microfracture; M, microfracture alone; N, normal cartilage; R, repair tissues. The arrows indicate the margins of the normal and repaired tissue. Scale bars=500 μm. Samples from the central part of the repaired tissue 24 weeks after transplantation were evaluated by a nanofindenter. Microscopic geomorphology of the repaired zone was acquired during nanoindentation (B). Reduced modulus (C), hardness (D) and contact stiffness (E) of the repair tissues were compared with the normal cartilage. Higher mechanical properties can be seen in the repair tissues in the ABM+M group. ABM, decalcified cortical-cancellous bone matrix; ABM+M, perforated ABM combined with microfracture; M, microfracture alone; N, normal cartilage. (n=9, *P<0.05).

niques, such as periosteal transplantation, osteochondral transplantation [17], and matrix-assisted chondrocyte implantation [18, 19]. All these problems significantly motivated researchers to find new approaches for cartilage repair.

Thus, we designed a method that first releases autologous cells by the marrow stimulation technique and then creates a favorable microenvironment by using the ABM scaffold for induction and formation of hyaline-cartilage.

This method can be performed in a one-step procedure and can utilize endogenous cells without donor site morbidity. Preliminary studies and the current study have confirmed that this technique is easy to perform and leads to hyaline-like cartilage repair [20, 21, 24].

Several factors may have contributed to the satisfactory results. First, cells induced by Microfracture can migrate to the cartilage defect region, while the ABM scaffold provides a microenvironment for cell survival and differentiation. Second, the porous structure of the ABM scaffold is conducive to the increase of cell growth and adhesion. Third, the ABM scaffold itself contains many proteins that may help with the regeneration of subchondral bone, induce cartilage differentiation, and stimulate cartilage matrix formation [25].

The optimal scaffold can attract cell attachment, proliferation, and differentiation [26]. The ABM scaffolds maintain a more natural 3D collagen structure, better cell permeability, better biological compatibility, and better mechanical properties compared with other non-biological materials, such as carbon fiber, collagen sponge, absorbing polymers, and hydroxyapatite [27-29]. It is suitable for cartilage repair regardless of the structure and biological prop-

erties. The cortical part (1 mm thick) facing the cartilage defect was used as a basic support. The demineralized cancellous parts served as the main body of the scaffold for cartilage regeneration. Drilling was performed for bone marrow stem cells to penetrate into the defect region. Moreover, the ABM scaffold is rich with bone morphogenetic proteins (BMPs) and a variety of cytokines that promote the induction of cartilage [30, 31] and the secretion of cartilage ECM, thereby playing an important role in the start of cartilage repair and shaping [32].

ECM-based engineering strategies are already being used clinically for other tissues, such as muscle, tendon [33], and heart valves [34].

The use of a natural, acellular matrix is a promising strategy for regenerative medicine and cartilage tissue engineering and can easily be translated to clinical applications.

Acknowledgements

This work was supported by the National Natural Sciences Foundation of China (81330040, 81601927) and China Postdoctoral Science Foundation (2014M550569). Beijing New-star Plan of Science and Technology, grant number 171100001117133.

Disclosure of conflict of interest

None.

Address correspondence to: Yingfang Ao and Xiaoqing Hu, Institute of Sports Medicine, Peking University Third Hospital, Beijing Key Laboratory of Sports Injuries, 49 North Garden Road, Haidian District, Beijing 100191, PR China. Tel: +86-10 82267390; Fax: +86-10 62010440; E-mail: Yingfang.ao@vip.sina.com (YFA); Tel: +86-10 82265731; Fax: +86-10 82265731; E-mail: huxiaoqingbd01@sina.com (XQH)

References

[1] Curl WW, Krome J, Gordon ES, Rushing J, Smith BP and Poehling GG. Cartilage injuries: a review of 31,516 knee arthroscopies. Arthroscopy 1997; 13: 456-460.

[2] Flanigan DC, Harris JD, Trinh TQ, Siston RA and Brophy RH. Prevalence of chondral defects in athletes' knees: a systematic review. Med Sci Sports Exerc 2010; 42: 1795-1801.

[3] Madry H, Kon E, Condello V, Peretti GM, Steinwachs M, Seil R, Berruto M, Engebretsen L, Filardo G and Angele P. Early osteoarthritis of the knee. Knee Surg Sports Traumatol Arthrosc 2016; 24: 1753-1762.

[4] Knutsen G, Drogset JO, Engebretsen L, Grontvedt T, Ludvigsen TC, Loken S, Solheim E, Strand T and Johansen O. A randomized multicenter trial comparing autologous chondrocyte implantation with microfracture: long-term follow-up at 14 to 15 years. J Bone Joint Surg Am 2016; 98: 1332-1339.

[5] Gudas R, Stankevicius E, Monastyreckiene E, Pranys D and Kalesinskas RJ. Osteochondral autologous transplantation versus microfracture for the treatment of articular cartilage defects in the knee joint in athletes. Knee Surg Sports Traumatol Arthrosc 2006; 14: 834-842.

[6] Safran MR and Seiber K. The evidence for surgical repair of articular cartilage in the knee. J Am Acad Orthop Surg 2010; 18: 259-266.

[7] Mundi R, Bedi A, Chow L, Crouch S, Simunovic N, Sibilsky Enselman E and Ayeni OR. Cartilage restoration of the knee: a systematic review and meta-analysis of level 1 studies. Am J Sports Med 2016; 44: 1888-1895.

[8] Christensen BB, Olesen ML, Lind M and Foldager CB. Autologous cartilage chip transplantation improves repair tissue composition compared with marrow stimulation. Am J Sports Med 2017; 45: 1490-1496.

[9] Solheim E, Hegna J, Inderhaug E, Oyen J, Harlem T and Strand T. Results at 10-14 years after microfracture treatment of articular cartilage defects in the knee. Knee Surg Sports Traumatol Arthrosc 2016; 24: 1587-1593.

[10] Case JM and Scopp JM. Treatment of articular cartilage defects of the knee with microfracture and enhanced microfracture techniques. Sports Med Arthrosc Rev 2016; 24: 63-68.

[11] Chawla A, Twycross-Lewis R and Maffulli N. Microfracture produces inferior outcomes to other cartilage repair techniques in chondral injuries in the paediatric knee. Br Med Bull 2015; 116: 93-103.

[12] Niemeyer P, Albrecht D, Andereya S, Angele P, Ateschrang A, Aurich M, Baumann M, Bosch U, Erggelet C, Fickert S, Gebhard H, Gelse K, Gunther D, Hoburg A, Kasten P, Kolombe T, Madry H, Marlovits S, Meenen NM, Muller PE, Noth U, Petersen JP, Pietschmann M, Richter W, Rolauffs B, Rhunau K, Schewe B, Steinert A, Steinwachs MR, Welsch GH, Zinser W and Fritz J. Autologous chondrocyte implantation (ACI) for cartilage defects of the knee: a guideline by the working group "Clinical Tissue Regeneration" of the German Society of Orthopaedics and Trauma (DGOU). Knee 2016; 23: 426-435.

[13] Saris DB, Vanlauwe J, Victor J, Haspl M, Bohnsack M, Fortems Y, Vandekerckhove B, Alm-

qvist KF, Claes T, Handelberg F, Lagae K, van der Bauwhede J, Vandenneucker H, Yang KG, Jelic M, Verdonk R, Veulemans N, Bellemans J and Luyten FP. Characterized chondrocyte implantation results in better structural repair when treating symptomatic cartilage defects of the knee in a randomized controlled trial versus microfracture. Am J Sports Med 2008; 36: 235-246.

[14] Zhang C, Cai YZ and Lin XJ. One-step cartilage repair technique as a next generation of cell therapy for cartilage defects: biological characteristics, preclinical application, surgical techniques, and clinical developments. Arthroscopy 2016; 32: 1444-1450.

[15] Kon E, Delcogliano M, Filardo G, Montaperto C and Marcacci M. Second generation issues in cartilage repair. Sports Med Arthrosc Rev 2008; 16: 221-229.

[16] Hettrich CM, Crawford D and Rodeo SA. Cartilage repair: third-generation cell-based technologies--basic science, surgical techniques, clinical outcomes. Sports Med Arthrosc Rev 2008; 16: 230-235.

[17] Hangody L, Dobos J, Balo E, Panics G, Hangody LR and Berkes I. Clinical experiences with autologous osteochondral mosaicplasty in an athletic population: a 17-year prospective multicenter study. Am J Sports Med 2010; 38: 1125-1133.

[18] Brittberg M. Cell carriers as the next generation of cell therapy for cartilage repair: a review of the matrix-induced autologous chondrocyte implantation procedure. Am J Sports Med 2010; 38: 1259-1271.

[19] Welsch GH, Mamisch TC, Zak L, Blanke M, Olk A, Marlovits S and Trattnig S. Evaluation of cartilage repair tissue after matrix-associated autologous chondrocyte transplantation using a hyaluronic-based or a collagen-based scaffold with morphological MOCART scoring and biochemical T2 mapping: preliminary results. Am J Sports Med 2010; 38: 934-942.

[20] Dai L, He Z, Zhang X, Hu X, Yuan L, Qiang M, Zhu J, Shao Z, Zhou C and Ao Y. One-step repair for cartilage defects in a rabbit model: a technique combining the perforated decalcified cortical-cancellous bone matrix scaffold with microfracture. Am J Sports Med 2014; 42: 583-591.

[21] Zhang X, Zheng Z, Liu P, Ma Y, Lin L, Lang N, Fu X, Zhang J, Ma K, Chen P, Zhou C and Ao Y. The synergistic effects of microfracture, perforated decalcified cortical bone matrix and adenovirus-bone morphogenetic protein-4 in cartilage defect repair. Biomaterials 2008; 29: 4616-4629.

[22] Huang H, Zhang X, Hu X, Shao Z, Zhu J, Dai L, Man Z, Yuan L, Chen H, Zhou C and Ao Y. A functional biphasic biomaterial homing mesenchymal stem cells for in vivo cartilage regeneration. Biomaterials 2014; 35: 9608-9619.

[23] Rafiq QA, Brosnan KM, Coopman K, Nienow AW and Hewitt CJ. Culture of human mesenchymal stem cells on microcarriers in a 5 l stirred-tank bioreactor. Biotechnol Lett 2013; 35: 1233-1245.

[24] Man Z, Hu X, Liu Z, Huang H, Meng Q, Zhang X, Dai L, Zhang J, Fu X, Duan X, Zhou C and Ao Y. Transplantation of allogenic chondrocytes with chitosan hydrogel-demineralized bone matrix hybrid scaffold to repair rabbit cartilage injury. Biomaterials 2016; 108: 157-167.

[25] Zhou S, Yates KE, Eid K and Glowacki J. Demineralized bone promotes chondrocyte or osteoblast differentiation of human marrow stromal cells cultured in collagen sponges. Cell Tissue Bank 2005; 6: 33-44.

[26] Sakata R, Iwakura T and Reddi AH. Regeneration of articular cartilage surface: morphogens, cells, and extracellular matrix scaffolds. Tissue Eng Part B Rev 2015; 21: 461-473.

[27] Hutmacher DW. Scaffolds in tissue engineering bone and cartilage. Biomaterials 2000; 21: 2529-2543.

[28] Kawazoe N, Chen G and Tateishi T. Development of novel biomaterials for bone and cartilage tissue engineering. Clin Calcium 2008; 18: 1713-1720.

[29] Ishimoto Y, Hattori K and Ohgushi H. Articular cartilage regeneration using scaffold. Clin Calcium 2008; 18: 1775-1780.

[30] Bessho K, Tagawa T and Murata M. Comparison of bone matrix-derived bone morphogenetic proteins from various animals. J Oral Maxillofac Surg 1992; 50: 496-501.

[31] Inoue T, Deporter DA and Melcher AH. Induction of chondrogenesis in muscle, skin, bone marrow, and periodontal ligament by demineralized dentin and bone matrix in vivo and in vitro. J Dent Res 1986; 65: 12-22.

[32] Gurevitch O, Kurkalli BG, Prigozhina T, Kasir J, Gaft A and Slavin S. Reconstruction of cartilage, bone, and hematopoietic microenvironment with demineralized bone matrix and bone marrow cells. Stem Cells 2003; 21: 588-597.

[33] Martinello T, Bronzini I, Volpin A, Vindigni V, Maccatrozzo L, Caporale G, Bassetto F and Patruno M. Successful recellularization of human tendon scaffolds using adipose-derived mesenchymal stem cells and collagen gel. J Tissue Eng Regen Med 2014; 8: 612-619.

[34] D'Onofrio A, Cresce GD, Bolgan I, Magagna P, Piccin C, Auriemma S and Fabbri A. Clinical and hemodynamic outcomes after aortic valve replacement with stented and stentless pericardial xenografts: a propensity-matched analysis. J Heart Valve Dis 2011; 20: 319-325; discussion 326.